Supplementary Materials for

Dysfunction of parvalbumin neurons in the cerebellar nuclei produces an action tremor

Mu Zhou, Maxwell D. Melin, Wei Xu, Thomas C. Südhof

Ten supplementary figures and five supplementary videos are provided in the supplementary materials.

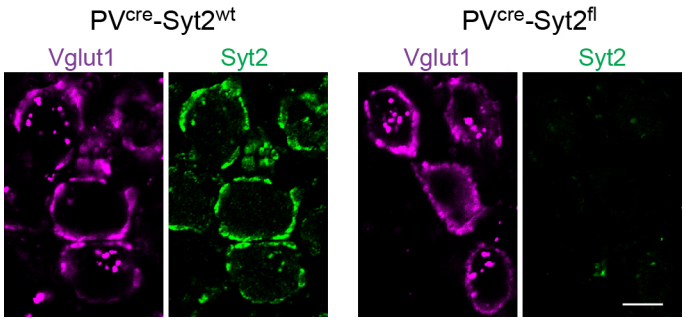

Supplementary Figure 1. Validation of PV^{cre}-$Syt2^{fl}$ mice

Representative immunostaining images of the Calyx of Held coronal section from PV^{cre}-$Syt2^{fl}$ and control mice showing the deletion of Syt2 from PV^{+} neurons. The Calyx synapses express Syt2 and are from PV^{+} bushy cells in the ventral cochlear nucleus. Vglut1 signal is used as the internal control. Scale bar: 10 μm.

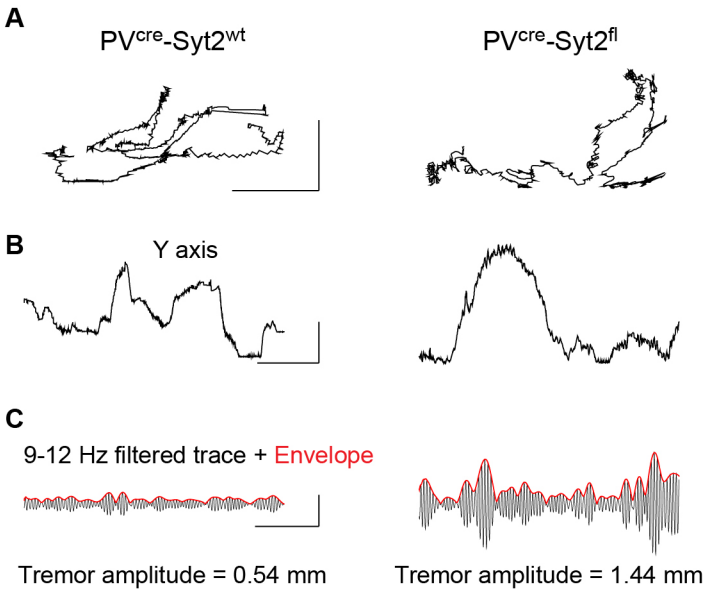

Supplementary Figure 2. Tremor quantification using video tracking.

(**A**) Moving trace of representative control (left) and PV^{cre}-Syt2^{fl} (right) mice's nose location during a 10 sec time window moving on the force plate. The nose location was retrieved with a video tracking software from the video captured with a high-speed camera (see methods). (**B**) The same data from **A**, showing moving trace on the Y-axis. (**C**) Bandpass-filtered (9-12 Hz) Y-axis moving trace. Calculated envelope is shown in red. Tremor amplitude was calculated as the average of envelope. Scale bars: 5 cm (**A** vertical); 5 cm (**A** horizontal); 3 cm (**B** vertical); 2 s (**B** horizontal); 2 mm (**C** vertical); 2 s (**C** horizontal).

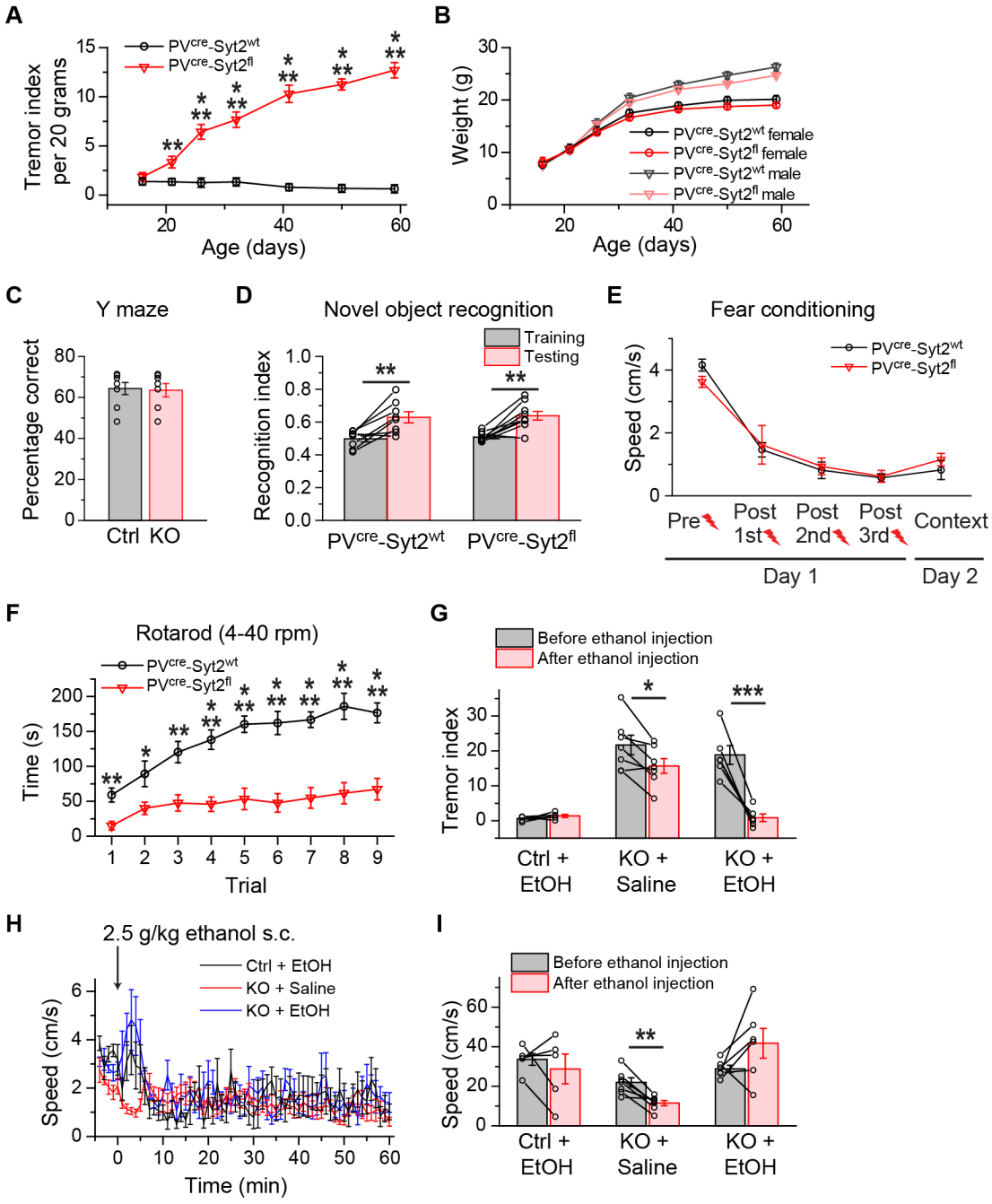

Supplementary Figure 3: Behavioral characterization of PV^{cre}-Syt2^{fl} mice.

(**A**) Summary plot of the tremor index per 20 grams of PV^{cre}-Syt2^{fl} and control mice as a function of age (n = 19 Control, n = 18 PV^{cre}-Syt2^{fl}). (**B**) Summary plot of the weight of PV^{cre}-Syt2^{fl} and control mice as a function of age (n = 10 Control female, n = 11 PV^{cre}-Syt2^{fl} female, n

= 9 Control male, n = 7 PV^{cre}-$Syt2^{fl}$ male). (**C** to **F**) Performance of control and PV^{cre}-$Syt2^{fl}$ (KO) mice in spontaneous alternating Y maze (**C**; n = 8 Control, n = 9 KO), novel object recognition test (**D**; n = 8 Control, n = 9 PV^{cre}-$Syt2^{fl}$), fear conditioning test (**E**; n = 6 Control, n = 5 PV^{cre}-$Syt2^{fl}$) and rotarod test (**F**; n = 9 Control, n = 7 PV^{cre}-$Syt2^{fl}$). In fear conditioning assay, the suppression of locomotion after the three foot shocks and during the contextual recall indicate the acquisition and retrieval of contextual fear memory. (**G**) Summary graph of the tremor index of PV^{cre}-$Syt2^{fl}$ and control mice before and after an s.c. injection of 2.5 g/kg ethanol, with PV^{cre}-$Syt2^{fl}$ mice injected with saline used as a further control (n = 5 control + EtOH, n = 7 KO + Saline, n = 6 KO + EtOH). The tremor index was calculated based on the −5 ~ 0 min and 0 ~ 5 min time window shown in Figure 1G. (**H**) Summary plot of the locomotion speed of PV^{cre}-$Syt2^{fl}$ and control mice as a function of time after an s.c. injection of ethanol, with PV^{cre}-$Syt2^{fl}$ mice injected with saline used as a further control (n = 5 control + EtOH, n = 7 KO + Saline, n = 6 KO + EtOH). (**I**) Summary graph of the locomotion speed of PV^{cre}-$Syt2^{fl}$ and control mice before and after an s.c. injection of 2.5 g/kg ethanol, with PV^{cre}-$Syt2^{fl}$ mice injected with saline used as a further control (n = 5 control + EtOH, n = 7 KO + Saline, n = 6 KO + EtOH). The tremor index was calculated based on the −5 ~ 0 min and 0 ~ 5 min time window shown in **H**. For **A**-**I**, data are shown as means ± SEM from at least 3 independent litters. $^{**}P < 0.01$, $^{***}P < 0.001$, two-sided unpaired t test (**A**); $^{**}P < 0.01$, two-sided paired t test (**D**); $^{*}P < 0.05$, $^{**}P < 0.01$, $^{***}P < 0.001$, two-sided unpaired t test (**F**); $^{*}P < 0.05$, $^{***}P < 0.001$, two-sided paired t test (**G**); $^{**}P < 0.01$, two-sided paired t test (**I**).

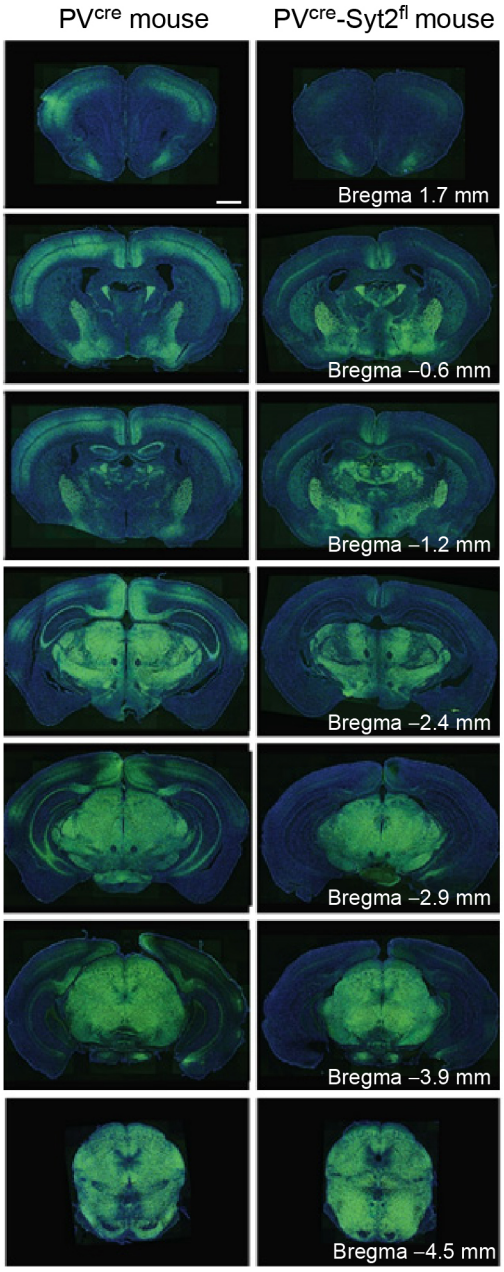

Supplementary Figure 4: Reduction of Syt2 expression in PV^{cre}-Syt2^{fl} mice.

Representative images of coronal brain sections showing the immunostaining of Syt2 for PV^{cre} (left) and PV^{cre}-Syt2^{fl} (right) mice in different brain regions. Images are arranged rostral to caudal from top to bottom. Scale bar, 1 mm.

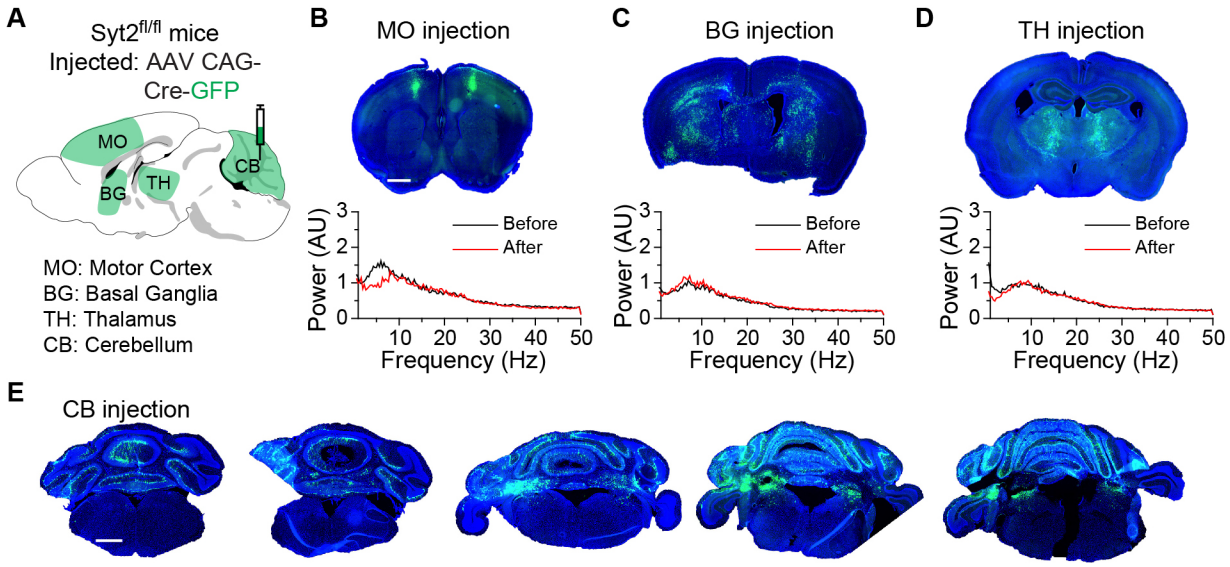

Supplementary Figure 5: Syt2 deletion from the cerebellum is sufficient to generate an action tremor.

(**A**) Stereotaxic injection strategy of AAVs encoding Cre-GFP into one of four brain regions: the motor cortex, basal ganglia, thalamus or cerebellum. (**B**) Top, a representative image showing the expressing of Cre-GFP in the motor cortex of Syt2$^{fl/fl}$ mice; Bottom, power spectrum of force plate measurements from the same mouse before and after viral injection. (**C** and **D**) The same as **B**, except the injections were performed in the basal ganglia (**C**) or the thalamus (**D**). (**E**) Representative images showing the expression of Cre-GFP in the cerebellum of the same Syt2$^{fl/fl}$ mice shown in Figure 3B. Images are arranged caudal to rostral from left to right. Scale bar, 1 mm (**B**). 1 mm (**E**).

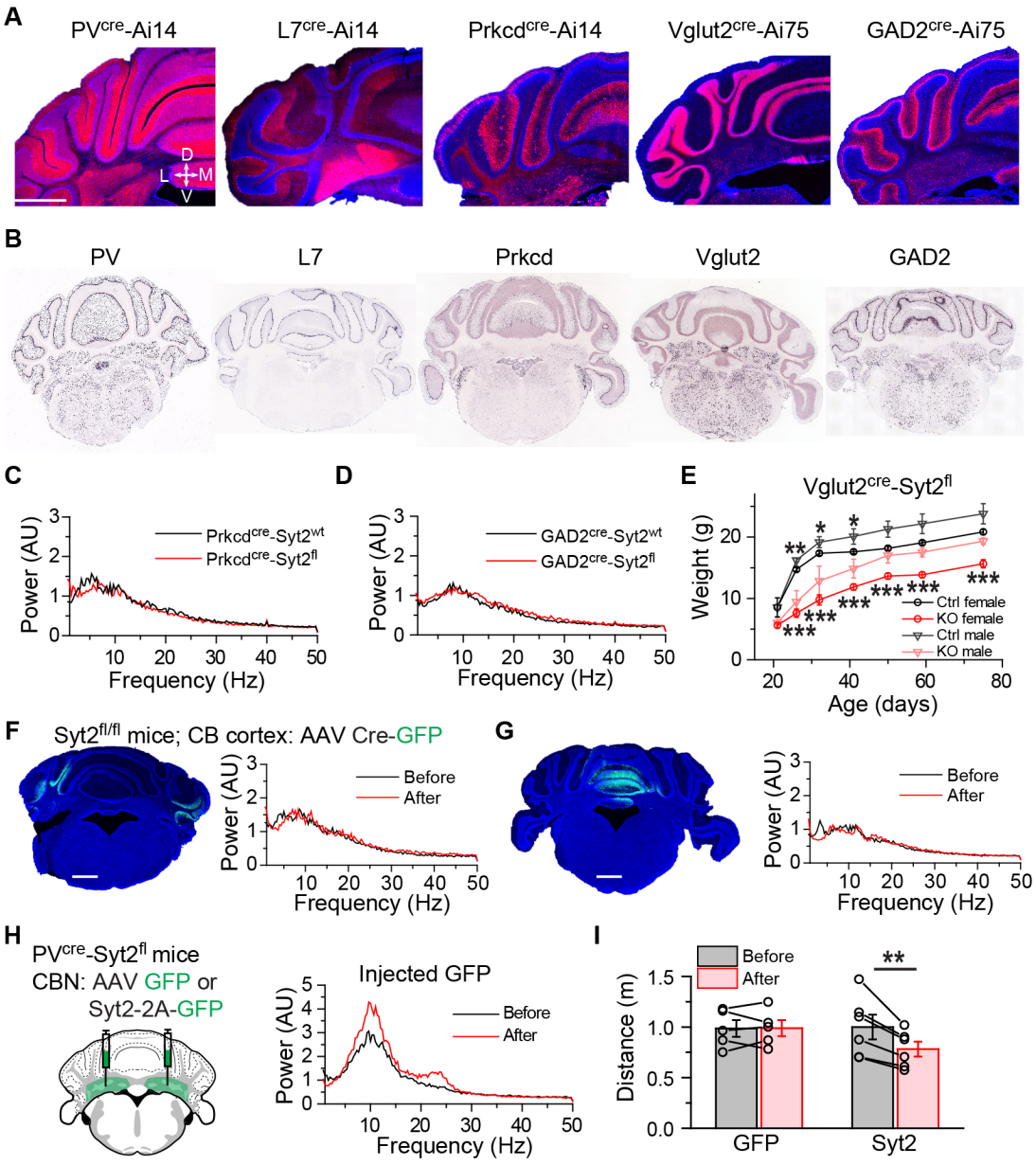

Supplementary Figure 6: Syt2 deletion from CBN PV^{+} neurons is sufficient to generate an action tremor.

(**A**) Representative images showing the cerebellar Cre expression patterns of PV^{cre}, L7^{cre}, Prkcd^{cre}, Vglut2^{cre} and GAD2^{cre} lines after crossing them with tdTomato reporter mice (Ai14 or Ai75). Note that in Ai14 reporter mice, tdTomato signals are in both soma and neurite. In Ai75 reporter mice, tdTomato signals are restricted to the nucleus. (**B**) Representative images showing

the in-situ hybridization results from Allen Mouse Brain Atlas for PV (experiment: 868), L7 (experiment: 77413702), Prkcd (experiment: 70301274), Vglut2 (experiment: 73818754) and GAD2 (experiment: 79591669) genes in the cerebellum. (**C** and **D**) Power spectra of force plate measurements from representative control and $Prkcd^{cre}$-$Syt2^{fl}$ mice (**C**) or control and $GAD2^{cre}$-$Syt2^{fl}$ mice (**D**). (**E**) Summary plot of the weight of $Vglut2^{cre}$-$Syt2^{fl}$ and control mice as a function of age (n = 9 Control female, n = 5 $Vglut2^{cre}$-$Syt2^{fl}$ female, n = 4 Control male, n = 3 $Vglut2^{cre}$-$Syt2^{fl}$ male). (**F**) Left, a representative image showing the bilateral expression of Cre-GFP in the lateral cerebellar cortex of a $Syt2^{fl/fl}$ mouse; Right, power spectrum of force plate measurements from the same Syt2 mouse before and after viral injection. (**G**) The same as **F**, except that the injections were made in the medial cerebellar cortex of a $Syt2^{fl/fl}$ mouse. (**H**) Left, stereotaxic injection strategy of AAVs encoding GFP or Syt2-2A-GFP into the CBN of PV^{cre}-$Syt2^{fl}$ mice; Right, power spectrum of force plate measurements from an example PV^{cre}-$Syt2^{fl}$ mouse before and after GFP overexpression. (**I**) Summary graph of moving distance in 5 min before and after GFP or Syt2 rescue expression in the CBN of PV^{cre}-$Syt2^{fl}$ mice (n = 5 GFP, n = 6 Syt2). For **E** and **I**, data are shown as means ± SEM from at least 3 independent litters. *P < 0.05, **P < 0.01, ***P < 0.001, two-sided unpaired t test (**E**); **P < 0.01, two-sided paired t test (**I**). Scale bars: 1 mm (**A**); 1 mm (**F**); 1 mm (**G**).

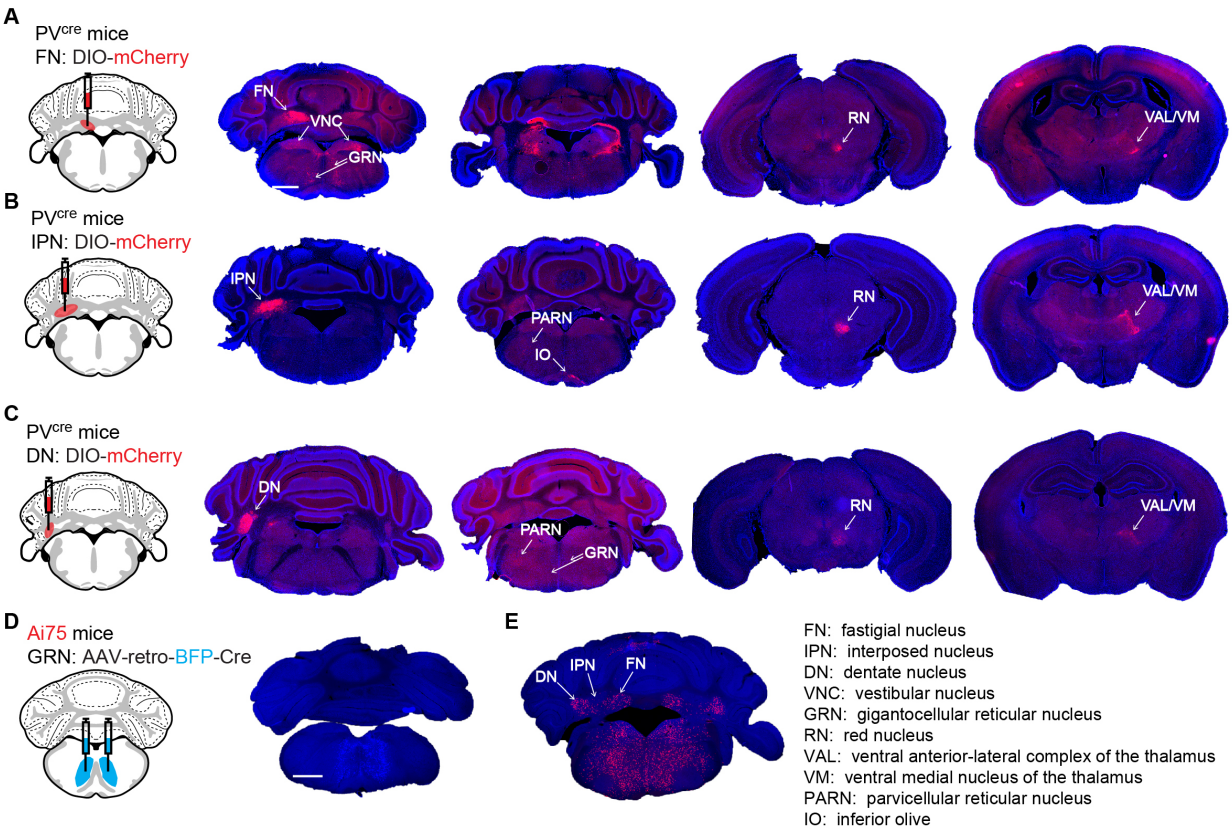

Supplementary Figure 7: Mapping of CBN downstream targets.

(**A**) Representative images of anterograde tracing experiments of projections from fastigial nucleus PV^{+} neurons to other brain regions (left, stereotactic injection strategy of AAVs encoding DIO-mCherry into the fastigial nucleus of a PV^{cre} mouse; right images, coronal slices arranged in a caudal → rostral direction showing mCherry expression in the indicated brain regions). (**B** and **C**) The same as **A**, except that tracing were from the interposed nucleus (**B**) and the dentate nucleus (**C**). (**D**) Left, stereotaxic injection strategy of AAV retro virus encoding blue fluorescence protein (BFP)-Cre into the GRN of an Ai75 mouse. Right, a representative image showing the injection site in GRN. (**E**) A representative image showing the retrogradely labelled neurons in the CBN. Note that most of the labelled neurons are in the dentate nucleus and fastigial nucleus. Scale bars: 1 mm (**A**); 1 mm (**D**).

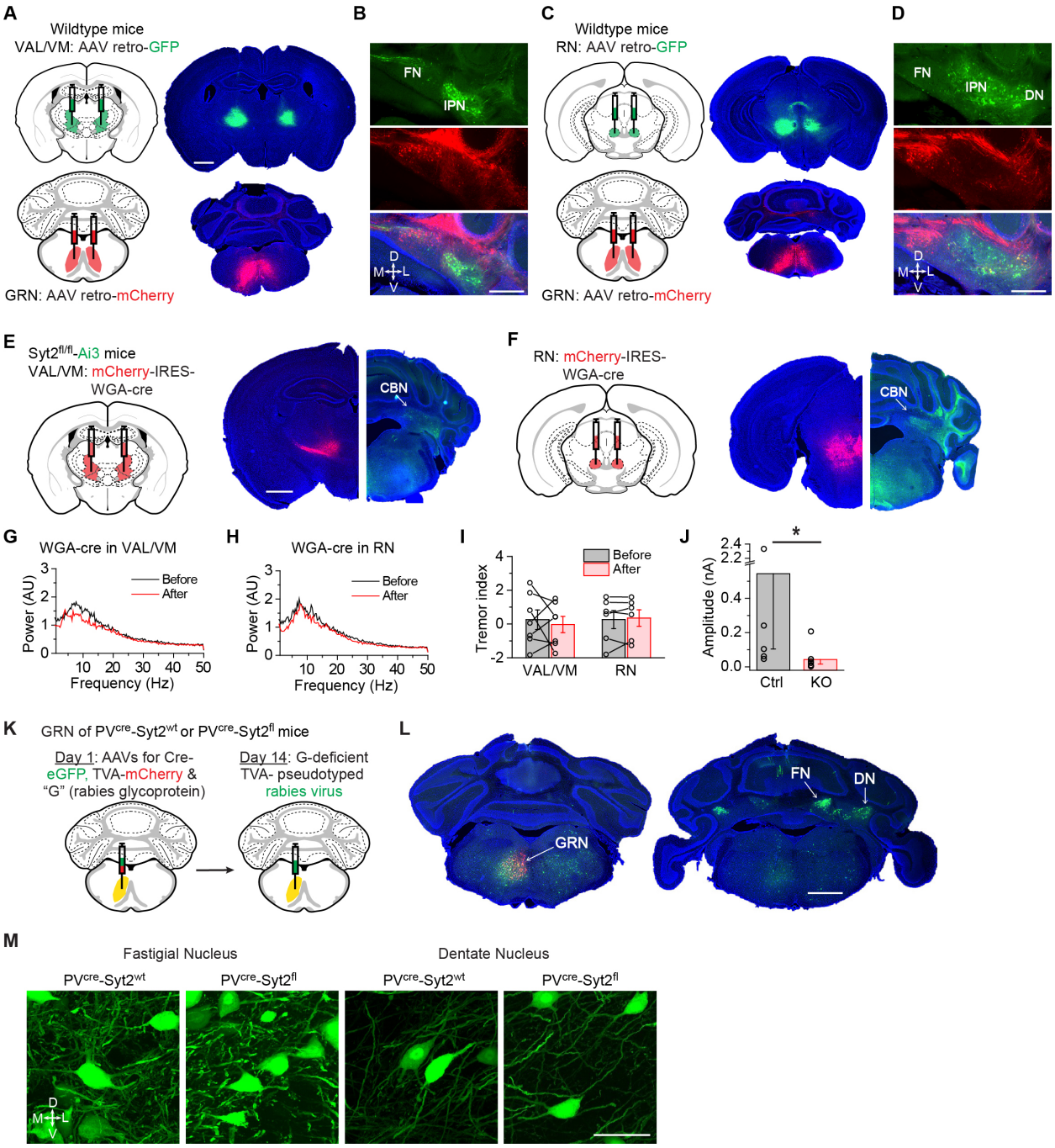

Supplementary Figure 8: Identification of CBN downstream targets that contribute to the action tremor.

(**A**) Left, stereotaxic injection strategies of AAV retro-GFP in the VAL/VM and AAV retro-mCherry in the GRN of a wildtype mouse. Right, representative images showing the

corresponding injection sites in VAL/VM and GRN. (**B**) Representative images showing the retrogradely labelled neurons in the CBN that project to the VAL/VM (green) and GRN (red). (**C** and **D**) The same as in **A** and **B**, except that AAV retro-GFP was injected in the red nucleus of a wildtype mouse. (**E** and **F**) Left, stereotaxic injection strategies of AAVs encoding mCherry-IRES-WGA-Cre in the VAL/VM (**E**) or red nucleus (**F**) of a Syt2-Ai3 mouse. Right, representative images showing the injection site and the retrogradely labelled neurons in the CBN. (**G** and **H**) Power spectrum of force plate measurements from the same Syt2-Ai3 mice shown in **E** and **F** before and 3 weeks after WGA-Cre injections. (**I**) Summary graph of the tremor index before and after WGA-Cre expression in the VAL/VM or red nucleus of Syt2-Ai3 mice (n = 7 VAL/VM, n = 6 RN). (**J**) Summary graph of the absolute amplitude of the first evoked EPSC response shown in Figure 5J (n = 5 Ctrl, n = 7 PV^{cre}-$Syt2^{fl}$). (**K**) Rabies virus tracing strategy. (**L**) Representative images showing the injection site and labelled neurons in the CBN. (**M**) Representative high resolution images showing the general morphology of GRN-projection neurons in the fastigial nucleus and dentate nucleus of control and PV^{cre}-$Syt2^{fl}$ mice. For **I** and **J**, data are shown as means ± SEM from at least 3 independent litters. *$P < 0.05$, Mann-Whitney test (**J**). Scale bars: 1 mm (**A**); 0.5 mm (**B**); 0.5 mm (**D**); 1 mm (**E**); 1 mm (**L**); 50 μm (**M**).

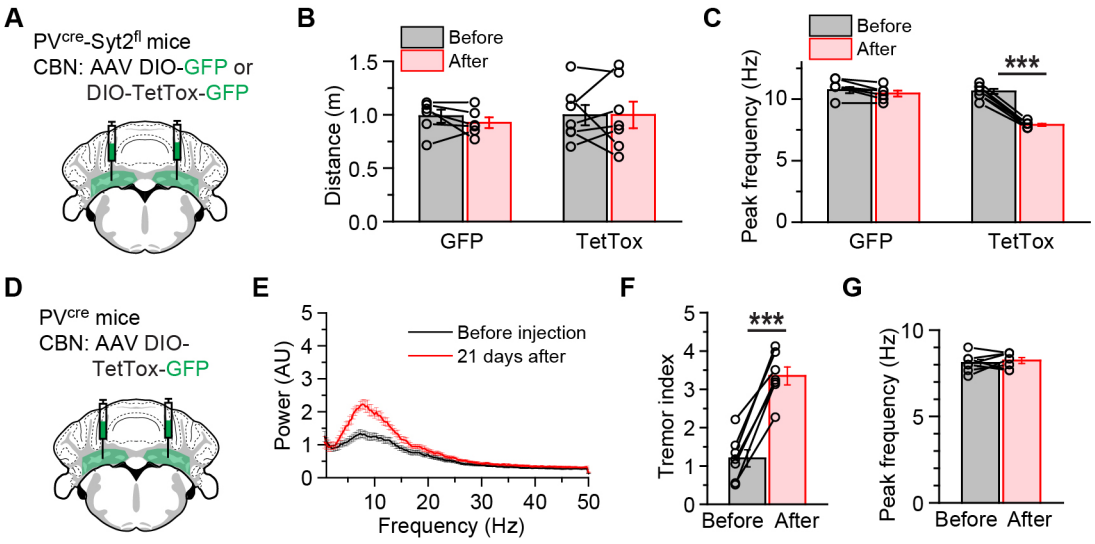

Supplementary Figure 9: Blocking neurotransmitter release in CBN neurons rescues the action tremor of PV^{cre}-Syt2^{fl} mice.

(**A**) Stereotaxic injection strategy of AAVs encoding DIO-GFP or DIO-TetTox-GFP into the CBN of PV^{cre}-Syt2^{fl} mice. (**B**) Summary graph of moving distance (5 min) before and after injection of AAVs encoding GFP or TetTox-GFP in the CBN of PV^{cre}-Syt2^{fl} mice (n = 6 GFP, n = 7 TetTox). (**C**) Summary graph of peak frequency (tremor frequency with largest power) before and after injection of AAVs encoding GFP or TetTox-GFP in the CBN of PV^{cre}-Syt2^{fl} mice (n = 6 GFP, n = 7 TetTox). (**D**) Stereotaxic injection strategy of AAVs encoding DIO-TetTox-GFP into the CBN of PV^{cre} mice. (**E**) Averaged power spectrum of force plate measurements from PV^{cre} mice before and after TetTox expression in CBN. Note that the tremor frequency after TetTox expression is similar to the physiological tremor frequency (n = 7). (**F**) Summary graph of tremor index before and after TetTox expression (n = 7). (**G**) Summary graph of peak frequency before and after injection of AAVs encoding TetTox-GFP in the CBN of PV^{cre} mice (n = 7). For **B**, **C**, **E-G**, data are shown as means ± SEM from at least 2 independent litters. ***P < 0.001, two-sided paired t test (**C**); ***P < 0.001, two-sided paired t test (**F**).

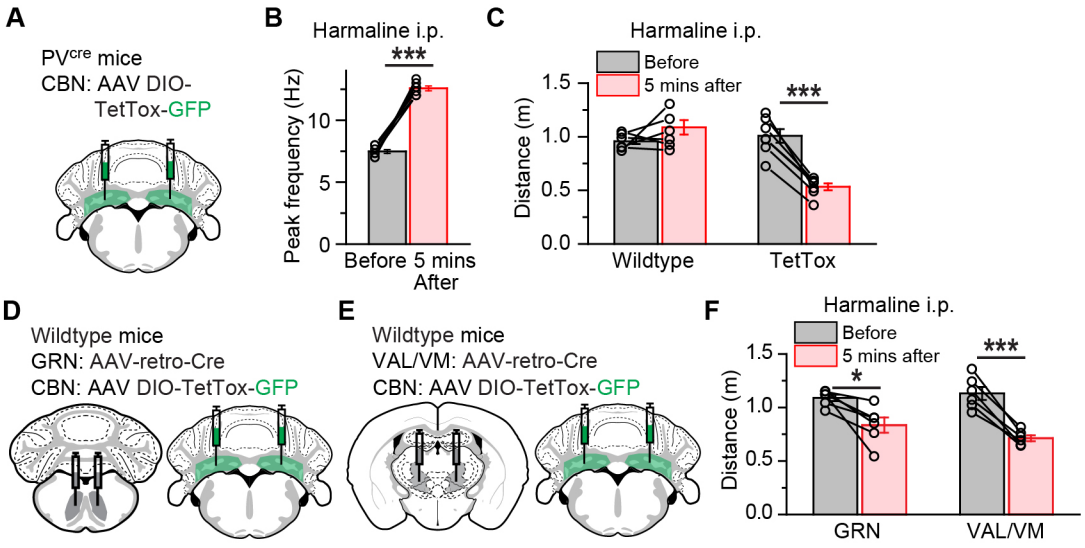

Supplementary Figure 10: Blocking neurotransmitter release in CBN neurons rescues the action tremor of harmaline-injected mice.

(**A**) Stereotaxic injection strategy of AAVs encoding DIO-TetTox-GFP into the CBN of PV^{cre} mice. (**B**) Summary graph of peak frequency before and 5 min after harmaline injection in wildtype mice (n = 7). (**C**) Summary graph of moving distance (5 min) before and 5 min after harmaline i.p. injection in wildtype and TetTox-injected mice (n = 7 Wildtype, n = 7 TetTox). Note that the harmaline i.p. injection and TetTox expression in CBN have a synergistic effect on suppressing locomotion. (**D** and **E**) Stereotaxic injection of AAV-retro-Cre in the GRN (D) or VAL/VM (E) and AAV DIO-TetTox-GFP in the CBN of wildtype mice. (**F**) Summary graph of moving distance (5 min) before and 5 min after harmaline i.p. injection in GRN- and VAL/VM-injected mice (n = 6 GRN, n = 6 VAL/VM). For **B**, **C** and **F**, data are shown as means ± SEM from at least 2 independent litters. ***$P < 0.001$, two-sided paired t test (**B**); ***$P < 0.001$, two-sided paired t test (**C**); *$P < 0.05$, two-sided paired t test (**F**); ***$P < 0.001$, two-sided paired t test (**F**).

Supplementary Movie 1. Quantification of tremor in an example PV^{cre}-$Syt2^{wt}$ mouse (PV +/–, Syt2 +/–) using both force plate and video tracking methods at the same time.

Supplementary Movie 2. Quantification of tremor in an example PV^{cre}-$Syt2^{fl}$ mouse (PV +/–, Syt2 –/–) using both force plate and video tracking methods at the same time.

Supplementary Movie 3. An example PV^{cre}-$Syt2^{fl}$ mouse showing significant tremor during locomotion.

Supplementary Movie 4. An example PV^{cre}-$Syt2^{fl}$ mouse showing robust freezing behavior during recall of contextual fear memory.

Supplementary Movie 5. An example $Syt2^{fl/fl}$ mouse showing the same action tremor symptoms as PV^{cre}-$Syt2^{fl}$ mice after expression of Cre recombinase in the whole cerebellum.